8-2019

An ANN-Based System for Lateral Misalignment and Vertical Clearance Estimation of an Electric Vehicle During Dynamic Wireless Charging

Sanat Kumar Saha
Utah State University

AN ANN-BASED SYSTEM FOR LATERAL MISALIGNMENT AND VERTICAL CLEARANCE ESTIMATION OF AN ELECTRIC VEHICLE DURING DYNAMIC WIRELESS CHARGING

by

Sanat Kumar Saha

A report submitted in partial fulfillment
of the requirements for the degree

of

MASTER OF SCIENCE

in

Electrical Engineering

Approved:

Zeljko Pantic, PhD Major Professor	Charles M. Swenson, PhD Committee Member

Jonathan Phillips, PhD
Committee Member

UTAH STATE UNIVERSITY
Logan, Utah

2019

ABSTRACT

AN ANN-BASED SYSTEM FOR LATERAL MISALIGNMENT AND VERTICAL CLEARANCE ESTIMATION OF AN ELECTRIC VEHICLE DURING DYNAMIC WIRELESS CHARGING

by

Sanat Kumar Saha, Master of Science

Utah State University, 2019

Major Professor: Zeljko Pantic, PhD
Department: Electrical and Computer Engineering

Due to decaying fossil fuel reserves, oil price fluctuation and detrimental effects on climate the use of fossil fuel has, people are getting more interested in other alternative energy sources. In the past couple of decades, the Electric Vehicles have emerged as a robust environment-friendly alternative to conventional gasoline-driven vehicles. Although EVs have a problem with the limited energy storage, Stationary and Dynamic Wireless Power Transfer (WPT) systems for the charging of EVs can be an effective solution. However, in a WPT system, energy efficiency and energy transfer capability are significantly affected by the level of Lateral Misalignment. The real-time estimation of LTM, followed by some corrective actions, could result in better energy efficiency and the power transfer capability of the system. This report describes the theory, design, and simulation of an Artificial Neural Network based system for predicting LTM and Vertical Clearance of EVs, so that the LTM can be corrected to optimize Wireless Power Transfer for EVs.

(49 pages)

PUBLIC ABSTRACT

AN ANN-BASED SYSTEM FOR LATERAL MISALIGNMENT AND VERTICAL CLEARANCE ESTIMATION OF AN ELECTRIC VEHICLE DURING DYNAMIC WIRELESS CHARGING

Sanat Kumar Saha

Due to decaying fossil fuel reserves, oil price fluctuation and detrimental effects on climate the use of fossil fuel has, people are getting more interested in other alternative energy sources. In the past couple of decades, Electric Vehicles (EV) have emerged as a robust environment-friendly alternative to the conventional gasoline-driven vehicles. Although EVs have a problem with the limited energy storage, Stationary and Dynamic Wireless Power Transfer (WPT) systems for the charging of EVs can be an effective solution. To implement wireless Power Transfer effectively, electric vehicles should be appropriately aligned over the charging pad. This research investigates, how well Artificial Neural Network can predict the lateral misalignment of the EV, comparing to the position of the primary charging pad so that the misalignment can be fixed to optimize Wireless Power Transfer.

To my parents for their relentless support throughout my entire life.

ACKNOWLEDGMENTS

I would like to thank Dr. Pantic for assisting me throughout the research. I would also like to thank my committee members, Dr. Swenson, Dr Phillips for their support and assistance throughout the entire process. I give special thanks to my family, friends and lab members specially Ujjwal Pratik, Reza Tavakoli, and Chakridhar Reddy Teeneti for their encouragement, moral support, and patience as I worked my way from the initial proposal writing to this final document. I could not have done it without all of you.

Sanat Kumar Saha

CONTENTS

Page

LIST OF TABLES

LIST OF FIGURES

ACRONYMS

WPT	Wireless Power Transfer
DWPT	Dynamic Wireless Power Transfer
LTM	LaTeral Misalignment
VC	Vertical Clearance
QL	Quality Factor
ITS	Intelligent Transportation Systems
DIS	Driver Information Systems
EV	Electric Vehicle
RMS	Root Mean Square
ANSYS	Analysis Systems (Simulation Software)

CHAPTER 1

INTRODUCTION

Throughout the last century, fossil fuel, such as petroleum or diesel, has been dominantly used for powering internal combustion engines in vehicles. However, due to public awareness of detrimental effects, such as global warming or air pollution, and due to the oil price fluctuation and the decaying fossil fuel reserves, people are getting more interested in other alternative energy sources. In the past couple of decades, Electric Vehicles (EV) have emerged as a robust environment-friendly alternative to conventional gasoline-driven vehicles. It is estimated that, by 2020, each major automobile company will release at least one EV model [1].

Stationary and Dynamic Wireless Power Transfer (WPT) systems for the charging of EVs can be an effective solution to the limited energy storage problem. For an adequate implementation of wireless charging, vehicles should be appropriately aligned over the charging pad. Unfortunately, as parking alignment significantly depends on drivers, only 5 percent of drivers park their vehicles within standard tolerances of inductive charging systems, leading to weak coupling between charging pads and inefficient wireless charging [2]. The problem gets even worse in dynamic charging systems due to continually changing position between transmitter and receiver pads. Here comes the importance of vehicle detection and correction before the vehicle reaches the charging pad.

The research report is part of *Design, Development, and Testing of a Dynamic Wireless Power Transfer (DWPT) System for Electric Vehicles* project at UPEL (Utah Power Electronics Lab). The project is divided into 3 phases. The objective of the first phase is to design, develop and demonstrate the operation of a down-scaled indoor DWPT test rig, where the power transmission is around 3.7 kW and the EV speed is limited to 3 m/s. The second phase will provide an outdoor system demonstration on a RAV4 Toyota vehicle where the power transfer is around 3.7 kW and the EV speed will be up to 50 km/h. During

the third and the final phase, the designed system for 30 kW DWPT system will be tested outdoor using the vehicle as the receiver. This project report describes one segment of the 1st phase of the entire project. The objective of this project segment is to use simulation data collected from the pad model to find the position and orientation of magnetic sensors that would result in minimum prediction error of the ANN algorithm. The sensor will be positioned at those optimum spots to provide the information about magnetic field to the ANN algorithm later. The research consists of three steps. During the first step, an ANSYS FEM model was built and simulated, and the magnetic field at each position surrounding the pad and for different vertical clearances was calculated. Second, the data was processed to create sets for training and verification of an Artificial Neural Network (ANN). In the third step, the ANN was trained to determine the sensor position and orientation that would predict LaTeral Misalignment (LTM) with a minimum estimation error. The very next step is to build a hardware platform to collect the data measured on the real hardware setup to repeat the training procedure, followed by ANN implementation and testing on experimental platform.

This research provides a tool that will be able to estimate the vehicle misalignment from the longitudinal axis of the charging pad, which will help the driver to correct the vehicle position comparing to the charging pad. Besides, it will help the charging controller to determine if the current flowing through the transmitter coil should be corrected, to provide expected power not only to well-aligned vehicles but to a misaligned vehicle, too.

CHAPTER 2

OBJECTIVE

Usually, a vehicle is detected by using road-embedded inductive loops [3], [4], but this method is costly, and it may have an impact on traffic flow. There are other methods for detecting/classifying vehicles where magnetic sensor measurements [5] are combined with Artificial Neural Network algorithms [6]. The efficiency of wireless power transfer of an EV depends not only on EV detection but also on the LTM comparing to the primary charging pad. [7] Shows how the transferred energy to the secondary/ receiving coil can be affected by LTM of the EV. The author demonstrated that the transferred energy reduces drastically if the normalized LTM of the EV becomes 0.5 (considering the width of the primary charging pad as reference). When the normalized LTM is 0.5, the transfered energy becomes almost half comparing to the energy transferred when there is zero LTM. To meet this low energy-transfer issue, it was proposed to increase the primary charging coil current depending on the size of LTM to maintain the same energy transfer. Although increment of the primary charging coil current helps the power-transferring system to maintain the same amount of energy transfer up to 0.5 normalized LTM, the efficiency of the power-transferring system decreases significantly due to the increment of primary charging coil current. Because of this, the detection of LTM is necessary before the EV reaches the primary charging coil and the correction of LTM is needed to minimize the system loss and optimize the efficiency of the wireless power transfer system.

At the top of it, the vertical clearance (height between EV-bottom pad and the primary charging coil) varies from vehicle to vehicle, which can affect the wireless power transfer, too. The idea is to train an Artificial Neural Network to identify the magnetic field pattern for lateral positions of different vehicle and different vertical clearances so that the proposed design can be used for various vehicles as the distance between the transmitting coil (charging pad) and receiving coil may vary depending on the size of the vehicle.

To summarize, the main objective of this project is to use simulation (with a high number of neurons to train Artificial Neural Network) data to find out the best suitable position and orientation for the magnetic sensors, so that the sensor structure can be implemented into hardware to accurately predict the LTM during dynamic wireless power transfer. Also, using the magnetic field pattern, EV would be detected before it reaches the primary charging coil. Since different EV has different vertical clearances, simulation data has been used to train ANN so that the trained network can detect different vertical clearances from the magnitude of the simulated magnetic field.

CHAPTER 3
LITERATURE REIVEW

3.1 Wireless Power Transfer (WPT)

Generally, the electrical wire is used to transfer electric power to electric- equipment. However, the use of wire is inconvenient for some cases, as the electrical equipment cannot move during powering and charging operation. Despite providing a mobile solution, the use of a battery has some limitations, such as the limited battery capacity, inconvenient charging process, high weight, and size. To avoid these issues, throughout the past few decades, WPT has been being developed, allowing power to be delivered without any contact between two objects by means of coupling magnetic field.

Inductive WPT can utilize magnetic material (typically ferrite) to enhance the coupling between pads, or it can be core-less. Both approaches have their advantages and deficiencies. For example, high power transfer capacity is one of the merits of using magnetic cores; on the other hand, the approach is expensive; it adds some additional weight and causes additional core losses. Therefore, magnetic cores are used where high-power transmission is required, while a core-less design is usually applied for low-power wireless transmission [8].

In general, a WPT system consists of a power-transmitting and power-receiving subsystems. Usually, the power-transmission part consists of a transmitter coil and an inverter, where the inverter energizes the transmitter coil. Magnetic flux, generated by the transmitter coil, transfers power to the receiver circuit. The power-receiving portion is comprised of a pick-up module and a regulator. The magnetic flux is received by the pickup module, and it produces power; on the other hand, the regulator controls the voltage and current of the pick-up module to stabilize the output power. Some power variation may occur due to the misalignment between the power transmission-part and the power-receiving part. In that case, the inverter can vary the current through the transmitter coil to regulate the output

power. On the power-receiving-side, the regulator may alter the effective quality factor of the resonant circuit at the receiver and that way allow power to be delivered [9].

3.2 LaTeral Misalignment (LTM)

In a Wireless Power Transfer system, LaTeral Misalignment (LTM) plays a significant role as the capability of energy transfer and energy efficiency depends on it. In order to improve energy transfer capability and achieve higher energy efficiency, real-time estimation and detection of LTM and remedial actions are needed. Drivers driving habits and road conditions may affect the amount of vehicle LTM; usually, for an average driver, the standard deviation of LTM is around 46 cm. Due to LTM, the expected received wireless power of an averaged sized vehicle may drop 46 percent compared to the power transfer of a vehicle with zero LTM [10]. Besides, the LTM is responsible for detuning of transmitter and receiver impedance matching networks, which may cause an additional drop in wireless power transfer.

Integration of complex tuning networks into compensation networks can sometimes mitigate the problem. Other possible options are increasing the current of the transmitter coil and changing loaded quality factor Q_L. However, changing Q_L comes with some negative consequences, e.g. the increase of the loss at the receiver due to high reactive current passing through the receiver compensation network; if the receiver reactance is not changed with the same scale as Q_L, the receiver side can cause detuning effect to the transmitter side; as VA requirement of the receiver compensation network elements is proportional to Q_L, it will also change [11]. For these reasons, real-time detection and correction of LTM are vital for the operation of a dynamic wireless power transfer system. Even if the driver action fails to reduce the misalignment, real-time control of the current of the transmitter coil can extend the nominal energy transfer zone for laterally misaligned vehicle [10].

3.3 Artificial Neural Network (ANN)

Fig 3.1 shows basic diagram of an Artificial Neural Network. An Artificial Neural Network is a data-processing pattern which is inspired by the way human nervous systems,

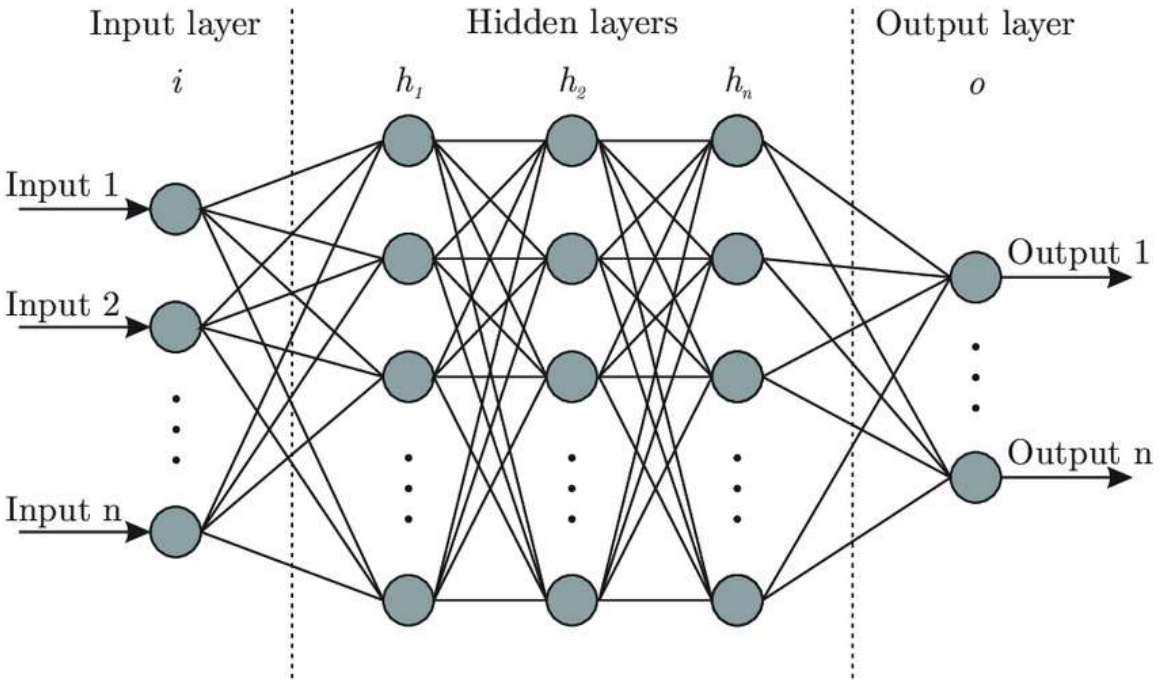

Fig. 3.1: Diagram of an Artificial Neural Network

processes information. The most significant part of this pattern is the structure of the information processing system which is a collection of many highly interconnected processing elements (neurons). They work together to solve specific problems by learning through examples. The problem-solving approach of conventional computers is different from the ANN approach. Computers use an algorithmic approach where it follows a set of instructions to solve a problem. If the specific steps that the machine needs to follow are unknown, the computer cannot solve the problem. This limits the problem-solving ability of computers to the problems that we already understand and know how to solve.

ANN is getting popularity for its Adaptive learning or capability to learn how to perform tasks based on the information given for training or initial experience and Self-Organization or capability of creating its organization or representation of the information it receives during the learning process. Since ANN computations may be carried out in parallel, specific hardware devices are being modeled and manufactured which take advantage of this capability. Another great feature of ANN is that the partial destruction of a network leads to the corresponding degradation of performance, but some network capabilities may

be retained even with a significant network damage [12].

A typical ANN consists of many artificial neurons (called units) arranged in a series of layers, where each layer connects to the layers on either side. Neurons from the first layer are known as input units which are designed to accept different forms of information that the ANN will try to learn or, recognize. The units situated on the other end of the network are known as output units, and their signal depends on how ANN responds to the information as it has learned. There are one or more layers of hidden units between the input units and output units, which, altogether, form most of the network. Most neural networks are entirely connected, which means that each hidden unit and each output unit is connected to every unit in the layers in both sides. The connection between each unit is represented by a number called weight, which can be either positive (if one unit excites another) or negative (if one unit suppresses or inhibits another). If the weight value of one unit goes higher, it has more influence has on another unit.

CHAPTER 4

METHODOLOGY

This chapter describes all design aspects of the project, starting from the visualization of the LTM detection system, ANSYS simulations, selection of the magnetic field, the collection of the data sequence for the ANN training purposes for the estimation of the LTM and vertical clearances. The objective of this section is to describe the complete procedure that was followed to obtain the optimum position for the sensors for the detection of the LTM. Here, simulations were used to figure out the best position of the sensors using ANN so that the detection system can be implemented.

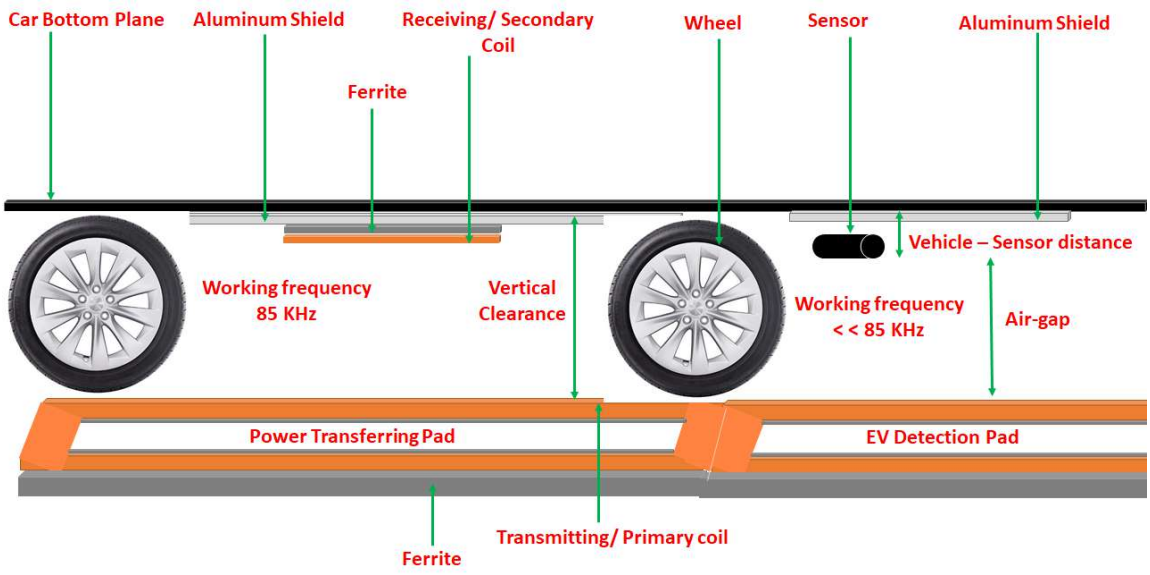

Fig. 4.1: Side view of an EV equipped with an LTM detection system.

Fig 4.1 shows side view of an EV where proposed LTM detection system has been implemented. The black horizontal line symbolizes the bottom of the car. The power transferring pad is embedded on the road, and multiple power transferring pad are situated next to each other along the length of the road. In the front part of the car-bottom side,

the main detection system is implemented. Three sensors are situated side by side to detect the magnetic field created by the primary charging coil. The car bottom is separated by aluminum shield so that the magnetic field created by the charging coil does not interfere with the car-bottom plane. When the detection system of EV enters a primary charging coil it is considered as EV detection pad, since the magnetic field generated by the charging pad is being only used for detection of the LTM.

The wireless power transfer system is situated between the two wheels of the EV and connected to the car chassis from the bottom. The power receiving coil is separated by Aluminum shield, and Ferrite is used to increase the magnetic coupling between the coils. The Primary charging coil is embedded on the road accompanied by Ferrite. The operating frequency is around 85 kHz for the wireless power transfer system. The total distance between the car-bottom plane and power transferring pad is called Vertical Clearance. The distance between the sensor and the car-bottom plane is called Vehicle-Sensor distance. Lastly, the distance between the sensor and the primary charging coil is called the Air-gap.

4.1 ANSYS-Simulation and Selection of the Magnetic Field

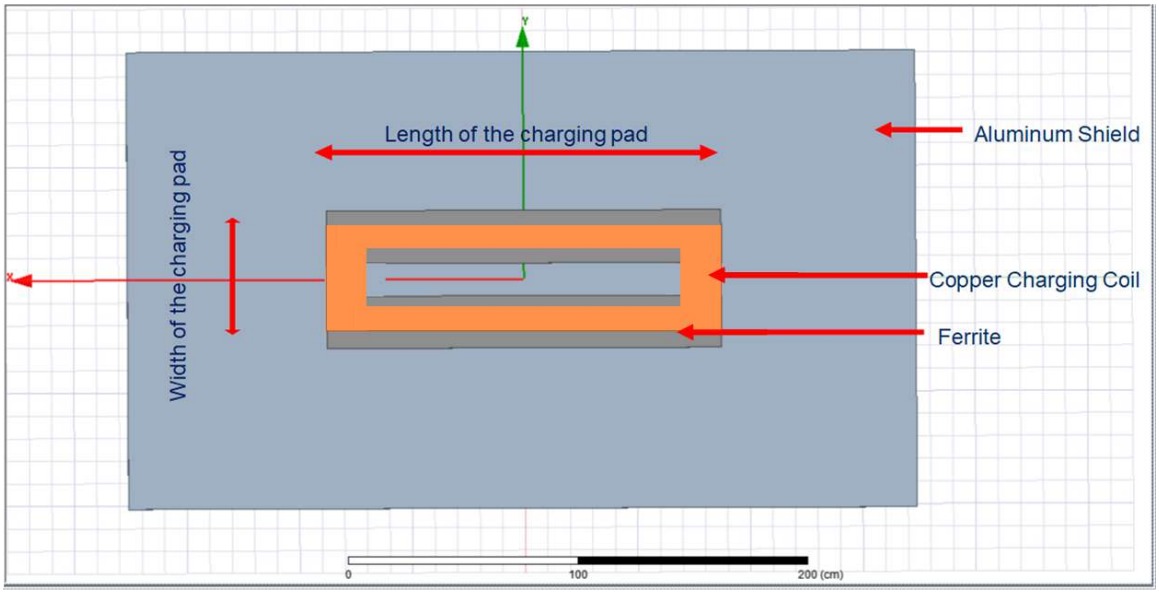

Fig. 4.2: ANSYS FEM model of the charging pad

Element	X-size (cm)	Y-size (cm)	Z-size (cm)
Aluminum Shield	350	202.4	0.5
Copper Charging Coil	175	50.6	0.632
Ferrite	175	61	0.25

Table 4.1: Measurements for ANSYS-simulation Model

The whole design for simulating the charging coil and calculation of the magnetic field was prepared in ANSYS. ANSYS is a simulation software that tests a models durability, temperature distribution, fluid movements, and electromagnetic properties, etc. Fig 4.2, top view of the model, shows the structure of the simulation model and position of the solid elements. Dark ash colored solid parts symbolize Ferrite which is in between of the Aluminum Shield and orange colored copper charging coil. There were total eight turns of the copper charging coil where each turn is separated by 0.76 cm along the length of the charging pad and by 2 cm along the width of the charging pad. As the current flowing through each coil was 5 Ampere, the total magnetomotive force of the charging pad was 40 Ampere-turns.

Table 4.1 shows appropriate measures of all solids (Aluminum Shield, Copper Charging Coil, and Ferrite) along the X, Y and Z axis. The Aluminum Shield was two times bigger in length and four times bigger in width comparing to the charging coil, which was designed to shield other components for hardware implementation from the magnetic field created by the charging coil. The distance between the Aluminum Shield and Copper Charging Coil varied due to different vehicle vertical clearance, which will be discussed later. The distance between two Ferrite bars from the charging pad was 0.5 cm which was situated along the length of the charging coil on both sides. The Ferrite bar was edging in from the innermost turn of the charging coil by 5.2 cm along the X-axis and edging out of the outermost turn of the charging coil by 5.2 cm along the Y-axis. The length of the Ferrite bars was the same as the length of the charging pad. The purpose of using the Ferrite bars was to attract the magnetic field lines around it to pass through it so that the intensity of the magnetic field gets higher for the ANSYS simulation.

4.1.1 Magnetic Field Along the Length of Charging Pad (Bx)

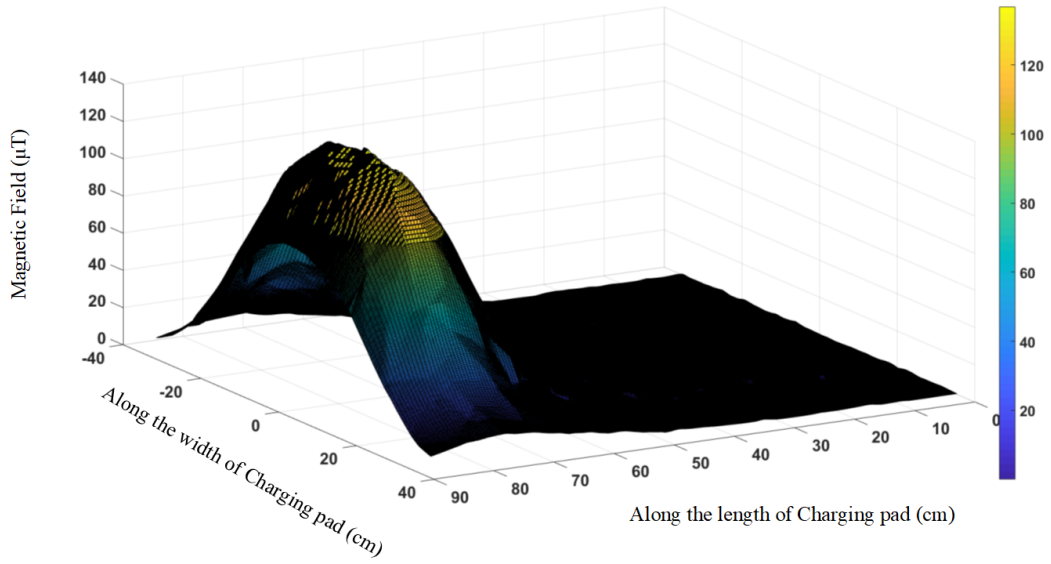

Fig. 4.3: 3-D plot of the Magnetic field (Bx) along the half-length of the charging pad.

Fig 4.3 demonstrates the magnetic field along the half-length of the charging pad (Bx). Here, central point of the charging pad is considered as the origin, and the edge of the charging pad is 87.5 cm as the total length of the charging pad is 175 cm. Due to the location of the coil at the beginning of the charging pad, significant Bx values can be observed only at the beginning. This is why there is a lump at the beginning of Fig 4.3. It was more evident when the contour of Bx was plotted in Fig 4.4, which illustrates the magnitude of Bx along with the half-length of the charging pad. Since except at the beginning of the charging pad, the magnitude of Bx of most of the simulation region was negligible, for simulation purpose, only the lump region was considered. Fig 4.5 shows the considered simulation region of the charging pad, where the magnitude of Bx is higher comparing to the rest of the charging pad. Another great advantage of considering this region is that, the while sensing the magnetic field, the magnetic sensors would be able to detect the big influx of Bx at the very beginning of the charging pad compared to the middle portion of the charging pad. This would help to detect the EV when it is entering the charging pad

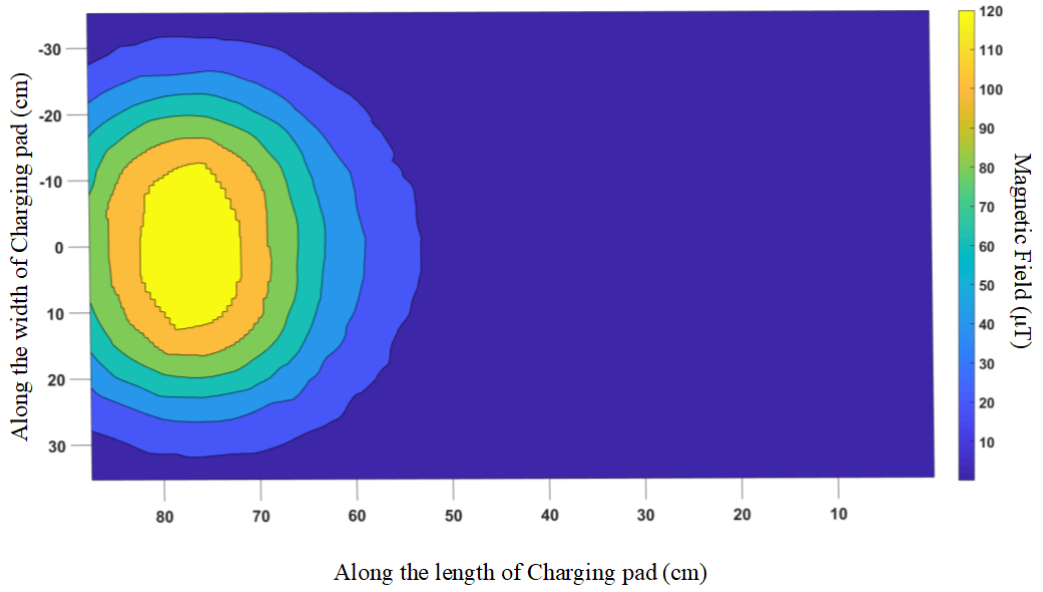

Fig. 4.4: Magnetic field (Bx) contour plot along the half-length of the charging pad.

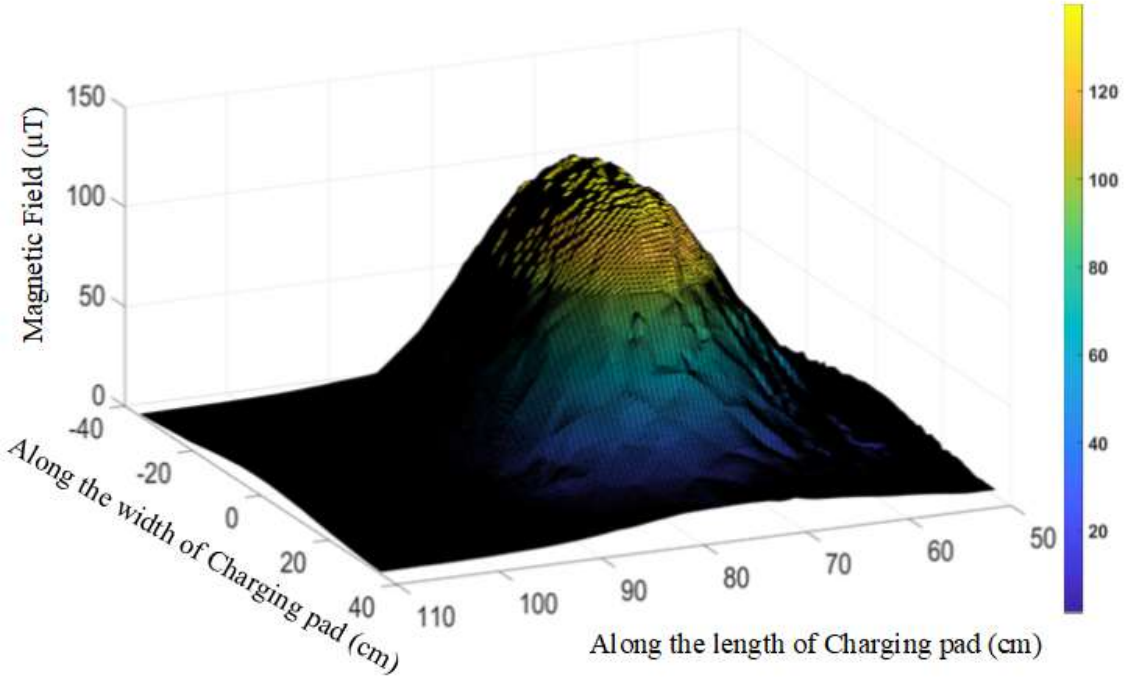

Fig. 4.5: 3-D plot of the selected Magnetic field (Bx) for ANN training.

area.

4.1.2 Magnetic Field Along the Width of Charging Pad (By)

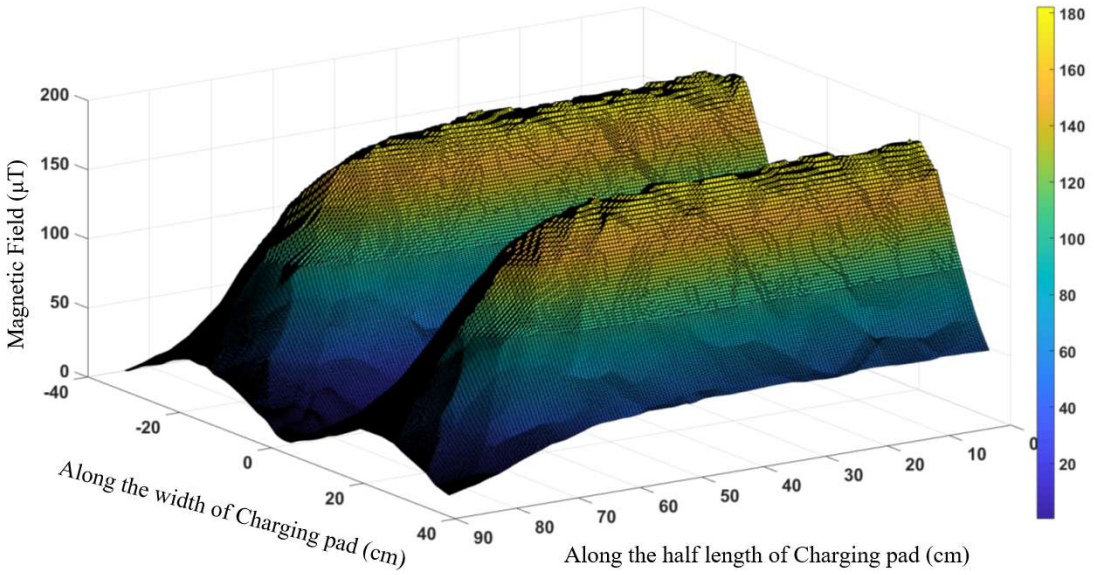

Fig. 4.6: 3-D plot of the Magnetic field (By) along the half-length of the charging pad.

The magnetic field along the Y-axis of the charging pad (By) throughout the half-length of the charging pad is illustrated in Fig 4.6. Since the charging coils are at the edge along the X-axis, the intensity of the magnetic field was higher compared to the middle of the charging pad. At the edge of the charging pad of the Y-axis, By is low since charging coil is aligned parallel to the Y-axis of the charging pad. Gradually the magnitude of By increases as the charging coil starts to align itself along the perpendicular of the Y-axis of the charging pad. Throughout the middle of the charging pad, it continues with almost a steady magnitude, making it difficult to detect the EV position on the charging pad. Fig 4.7

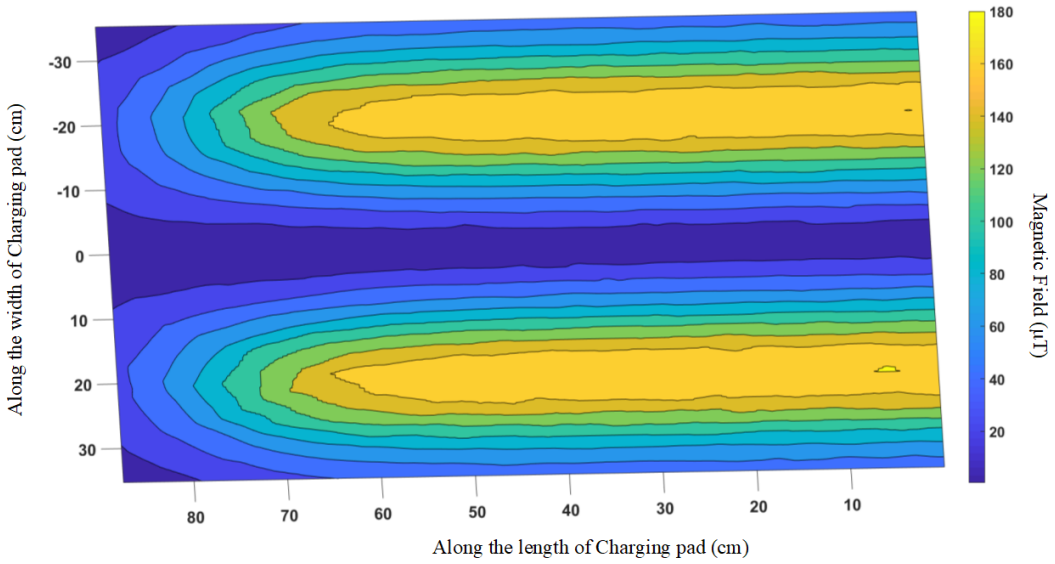

Fig. 4.7: Magnetic field (By) contour plot along the half-length of the charging pad.

is the contour plot for By, which shows that the magnitude of By is highest at those places above the charging coils.

4.1.3 Magnetic Field Along the Length of Charging Pad (Bz)

Fig 4.8 shows the magnitude of the simulated magnetic field along the Z-axis (perpendicular to the charging coil). As Aluminum Shield was used, it creates eddy current throughout the whole Aluminum pad. As a result, it interferes with the magnetic field created along the Z-axis causing fluctuation in the magnitude of the magnetic field throughout the entire charging pad. It is comprehensible from this figure that the magnetic field along the Z-axis (Bz) does not have any specific pattern. Since ANN cannot predict well when input data is incoherent, any calculation regarding Bz was avoided throughout the ANN training.

4.2 Training Artificial Neural Network

Fig 4.10 shows the complete flowchart of the ANN training and estimation procedure. The first step is to collect the magnetic field data points and store appropriately for MAT-

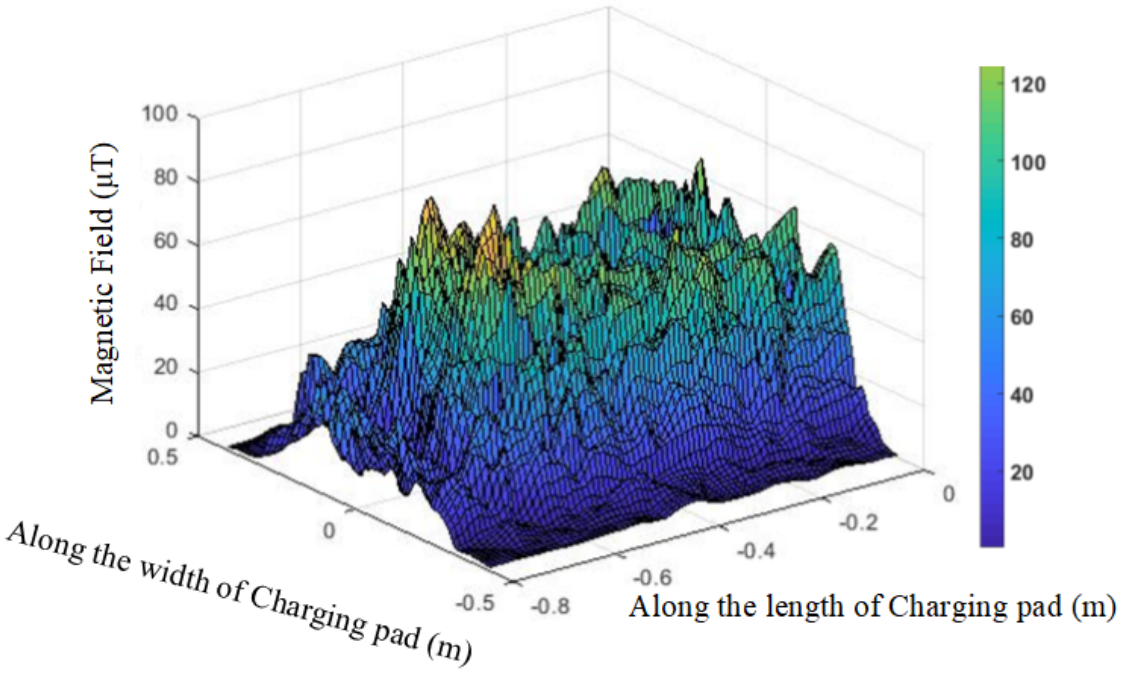

Fig. 4.8: Magnetic field (Bz) along the charging pad for simulation.

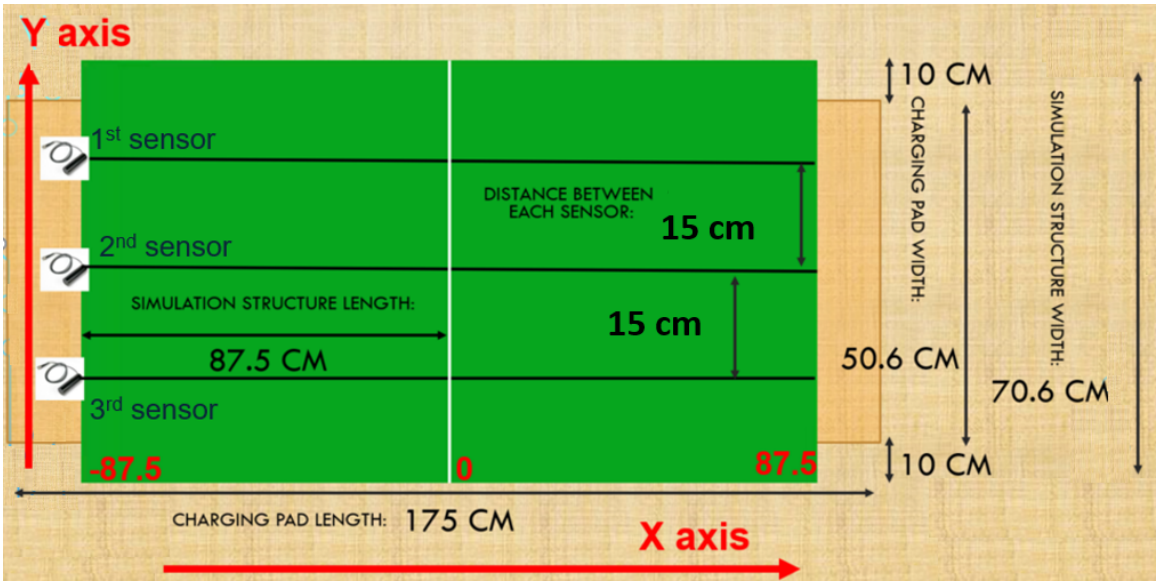

Fig. 4.9: Top view of the simulation region with measurements

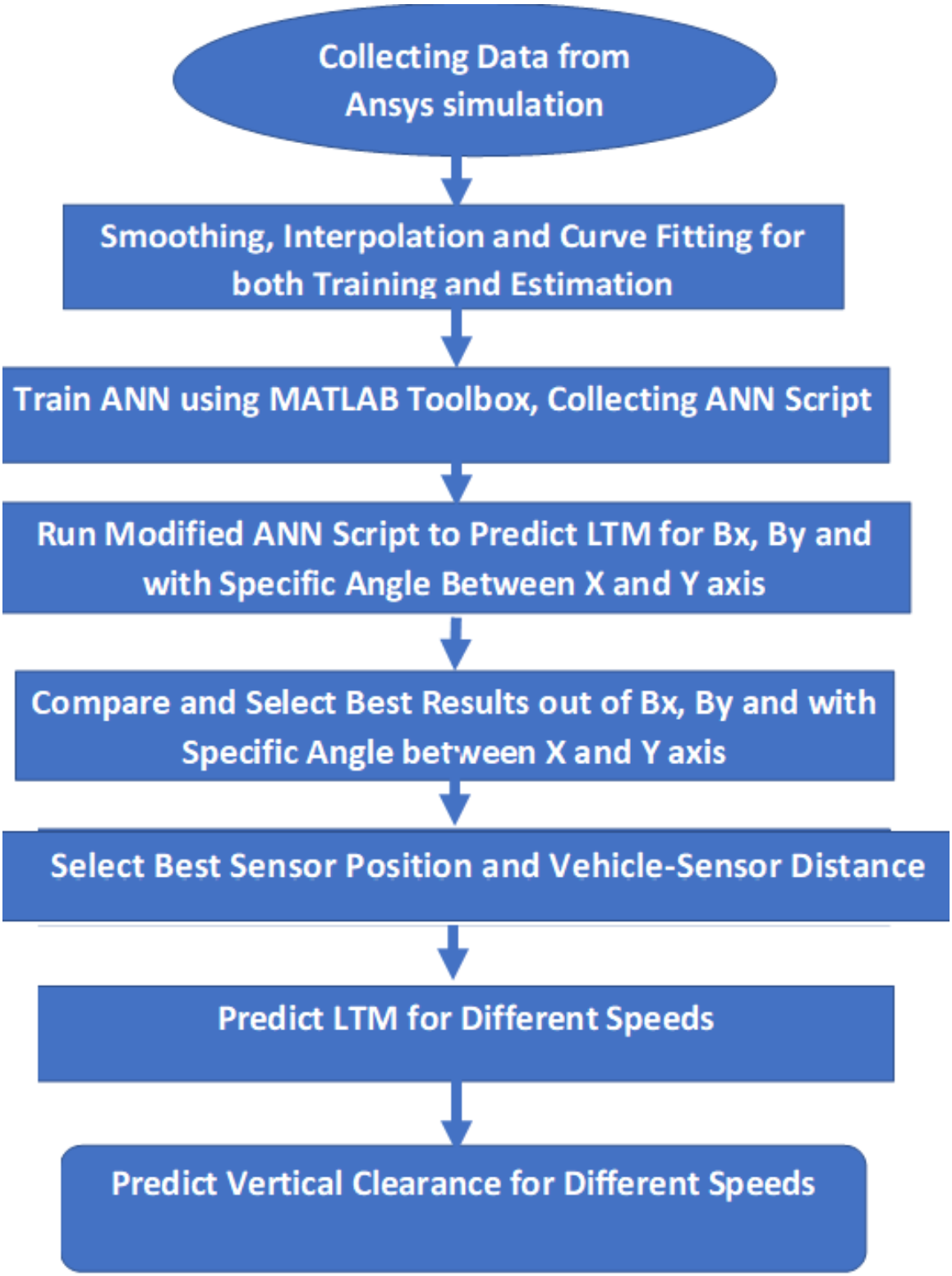

Fig. 4.10: Flowchart of training ANN and estimation of LTM and VC

LAB simulation. The received magnetic field curves throughout the simulation region were not smooth. Since ANN cannot predict well when the data is incoherent, the magnetic field curves were smoothed out by smoothing and interpolation. Using MATLAB curve fitting app, curves were fitted to the closest match for their quadratic equation for the best result. As it has been already discussed that Bz value is incoherent and unpredictable, it was omitted for ANN training. Therefore, for training ANN, only Bx or By was considered. Later, results of detection of LTM when sensors have specific angles with respect to the X-axis, was also determined. Results of detection of LTM for different Vehicle-Sensor Distance (distance between Vehicle bottom and Sensor) and different lateral positions of the sensors were also covered.

Fig 4.9 shows the initial setup of sensor position for training of ANN, where the 2nd sensor was in the middle and both 1st and 3rd sensor were 15 cm away from the 2nd sensor, and the 2nd sensor is in the middle of the charging pad. The magnetic flux density points were collected for the three sensors, along the X-axis for a specific position where the Air-gap was 11 cm, and Vehicle-Sensor Distance was 2 cm. The magnetic field points along the length of the charging pad for this combination of three sensors were considered as zero-misalignment. Then the whole setup was moved every half cm in both lateral directions (right and left along the Y-axis) where the distance between the sensors remained the same. The magnetic field data points for the corresponding lateral movement to the right of the charging pad was assigned to the corresponding misalignment value and considered as positively misaligned. For example, when the whole structure of sensors was moved 1 cm to the right side from the middle of the charging pad laterally (along with the Y axis), the magnetic field data points collected for three sensors were considered as magnetic flux density data points for +1cm positive misalignment. In a similar way, when the setup was moved to the left side from the middle of the charging pad along the Y-axis, it was considered as negative misalignment, and the specific magnetic flux density setup was assigned to their corresponding movement from the middle of the charging pad. The complete structure was capable of measuring 17 cm misalignment in both right and left side laterally from the

middle of the charging pad where the middle line of the charging pad along the X-axis is considered as the reference point. Since the complete setup was moved every half cm in both right and left side along the Y-axis, there were total 69 misalignment points, where one misalignment structure was for zero-misalignment (the reference), 34 misalignment points composition for positive misalignment and rest of them were for negative misalignments.

After collection of the magnetic flux density data, the next step was to train the ANN using MATLAB Neural Network Fitting app. The goal of using MATLAB Neural Network Fitting app was to create a neural network to map between a data set of numeric inputs and a set of numeric targets. A two-layer feed-forward network with sigmoid hidden neurons and linear output neurons can fit multi-dimensional mapping problems arbitrarily well, given consistent data and enough neurons in its hidden layer. The ANN was trained with Levenberg-Marquardt back-propagation algorithm, even though it needs more data points to predict the set of numeric targets. The network was trained with a different number of neurons, and also a different number of delays were introduced to observe how much the prediction results were affected by the different number of neurons and delays. The input for the ANN training was the set of magnetic sensor values concatenated for all the different misalignment points, and the ANN-target was the corresponding misalignments (in cm) concatenated corresponding to their magnetic flux density values.

CHAPTER 5

ANALYSIS OF THE RESULTS

The purpose of this project was to design and develop an ANN-based algorithm for estimating LTM and Vertical Clearance in order to implement the algorithm into hardware. This Section discusses the results for LTM estimation, Vertical Clearance prediction, and how the estimation of LTM is effected by speed, sensor position, angle of the sensor and Vehicle-Sensor Distance.

5.1 Testing Artificial Neural Network

After training the network, the code for manual training was extracted and implemented in a MATLAB code. In order to observe how the trained network performs, testing ANN code was developed. The whole procedure was similar to the Training code, except the fact that the complete sensor structure was moved every 0.1 cm instead of 0.5 cm. As a result, the total number of testing misalignment points for LTM prediction was 341, comparing to the number of training misalignment points of 69. For testing the trained network, one misalignment structure was for corresponds to zero-misalignment (the reference), 170 misalignment points composition for positive misalignment and the rest of them were for negative misalignment.

A total number of 60 misalignment points were selected covering the range of -17

Number of Delay: 1										
Number of Neurons	1	2	3	4	5	6	7	8	9	10
Mean of RMS LTM Prediction Error (cm)	2.29	1.43	0.87	0.76	0.67	0.56	0.51	0.45	0.42	0.35
Number of Delay: 5										
Number of Neurons	1	2	3	4	5	6	7	8	9	10
Mean of RMS LTM Prediction Error (cm)	2.27	1.21	0.81	0.73	0.66	0.56	0.50	0.44	0.39	0.33
Number of Delay: 10										
Number of Neurons	1	2	3	4	5	6	7	8	9	10
Mean of RMS LTM Prediction Error (cm)	2.26	1.41	0.79	0.68	0.62	0.49	0.47	0.39	0.36	0.31

Table 5.1: Effect of Number of Delays and Number on Neurons on average of RMS LTM estimation error

cm to +17 cm misalignment, and the average of the LTM prediction error was calculated for the chosen sixty misalignment points. The misalignment points were chosen up to one decimal point (for example -14.3 cm misalignment, -5.7 cm misalignment, +11.6 cm misalignment) covering the range of -17 cm to +17 cm. The sixty misalignment points that were selected from the ANN testing code were not included in the training ANN code to observe how accurately the ANN can predict different misalignment points where the data were not included in the training code. In order to calculate the average of the RMS LTM prediction error, estimation results for different points (along the X-axis), for one specific misalignment point were collected. Then RMS of LTM estimation were calculated for that particular misalignment point. After that, the RMS LTM estimation was deducted from that specific misalignment point to calculate the RMS LTM estimation error for that particular misalignment point. The same procedure was followed for the selected sixty misalignment points to calculate the RMS LTM estimation error for all the sixty misalignment points. Finally, the sum of all the RMS LTM prediction error was averaged to calculate the average of the LTM prediction error.

Also, the effect of different number of delays and neurons were calculated on ANN prediction. Table 5.1 demonstrates the effect of the number of neurons and delays on the precision of the estimation of LTM. If the number of neurons is increased, the average of RMS LTM prediction error reduces significantly, but it takes more time to train because of the increased number of coefficients needed for LTM estimation. The number of delays represents the number of consecutive magnetic flux density points were introduced to the training. Here, delay-1 is assigned as the number of delay elements, that means only one data point is provided for training. Since ANN can predict more precisely when the input is coherent, the increased number of delay provides better results for the estimation of LTM. However, results for the different number of delays were not significantly affecting the average of RMS LTM estimation error comparing to the results for the different number of neurons.

5.2 Orientation of the Optimum Position of the Sensing Devices

For first Training ANN and LTM estimation, only Bx was used, and the Vehicle-Sensor Distance (Fig 5.8) was selected to be 2 cm. The 2nd sensor was in the middle of the charging coil and both 1st and 3rd sensor was 15 cm apart from the 2nd sensor. Fig 4.9 shows the top view of the simulation region including sensor positions and proper measurements. In this section, three topics are discussed; Selection of Lateral Position of the Sensors, Sensor Positions with Different Angles with X-axis, and Selection of the Vehicle-Sensor Distance (distance between the EV bottom pad and the sensor).

5.2.1 Selection of Lateral Position of the Sensors

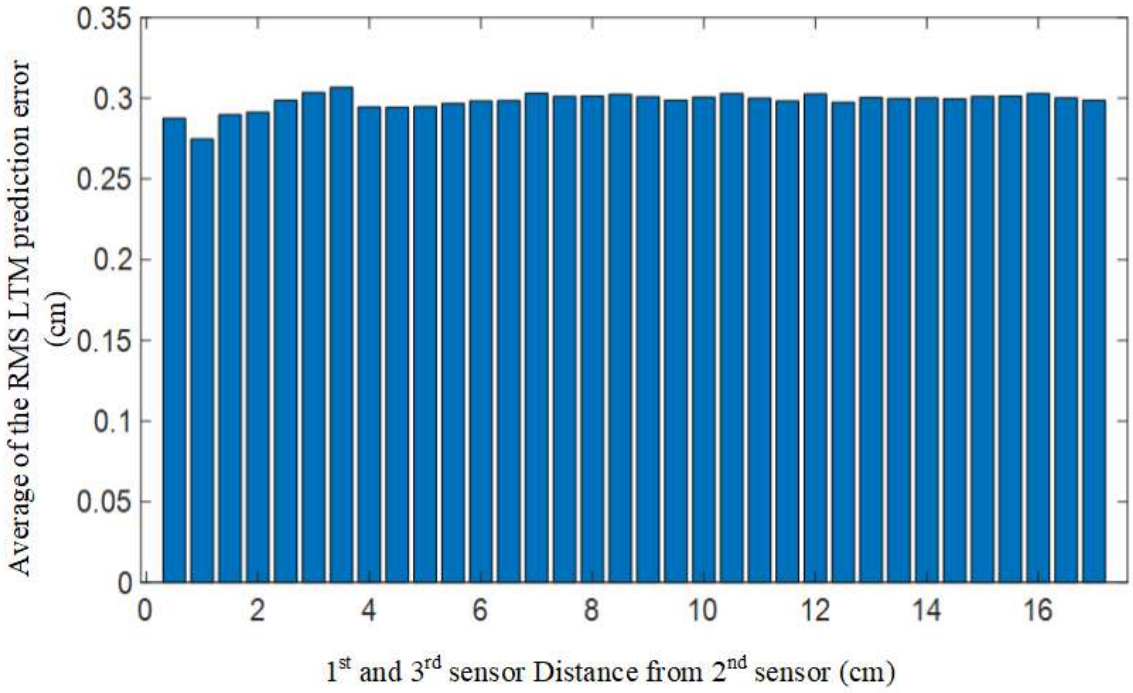

Fig. 5.1: Average of the RMS LTM prediction error when the 1st and the 3rd sensors are moving equidistantly from the 2nd sensor

For the selection of the appropriate Lateral Position of the Sensors, the 2nd sensor was kept in the middle of the charging pad facing the length of the charging pad. Both the 1st sensor and the 3rd sensor were moved every half cm equidistantly from the 2nd sensor

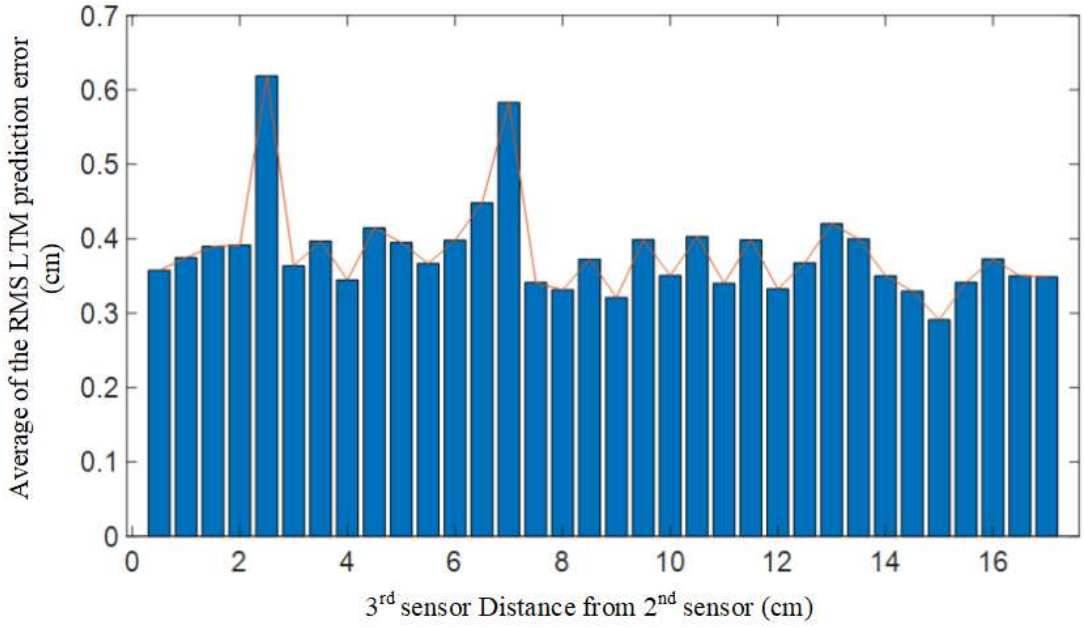

Fig. 5.2: Average of the RMS LTM prediction error when only the 3rd sensor is moving from the 2nd sensor and the 1st sensor is fixed (15 cm away from the 2nd sensor); number of neurons used for training is ten/hidden layer

to create a symmetrical sensor position. To assign the magnetic field to its corresponding misalignment values, the whole set of 3 sensors were shifted to the right in order to assign positive misalignment, and to the left to assign negative misalignment. The structure could estimate up to 17 cm misalignment in both directions. Fig 5.1 shows that results of the average of the LTM prediction error when both the 1st sensor and the 3rd sensor is moving equidistantly from the middle sensor. It can be clearly shown that the of the average of RMS LTM prediction error does not change much due to the change of the sensor positions. This indicates an important supposition that the estimation of LTM provides an optimum result when sensor positions are symmetrical and do not depend on how far the 1st and the 3rd sensors are located from the 2nd sensor if they are balanced. Since symmetrical sensor position does not make any impact on the LTM estimation, 15 cm was chosen for the distance from the 2nd sensor to both the 1st sensor and the 3rd sensor.

Then, the position of the 1st and the 2nd sensor was kept stationary, and only the 3rd sensor was moved every half cm. Then, the average of the LTM estimation error was

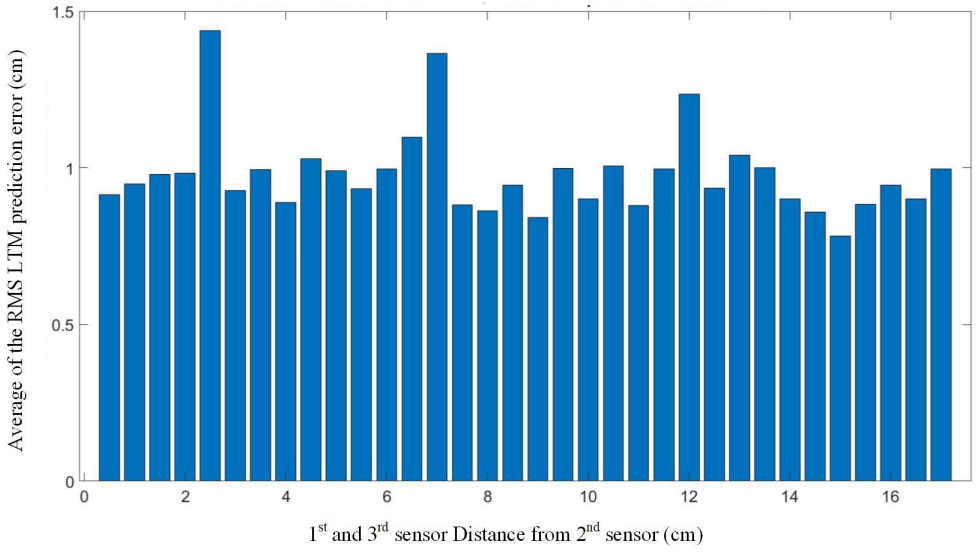

Fig. 5.3: Average of the RMS LTM prediction error when only the 3rd sensor is moving from the 2nd sensor and the 1st sensor is fixed (15 cm away from the 2nd sensor); number of neurons used for training is four/hidden layer

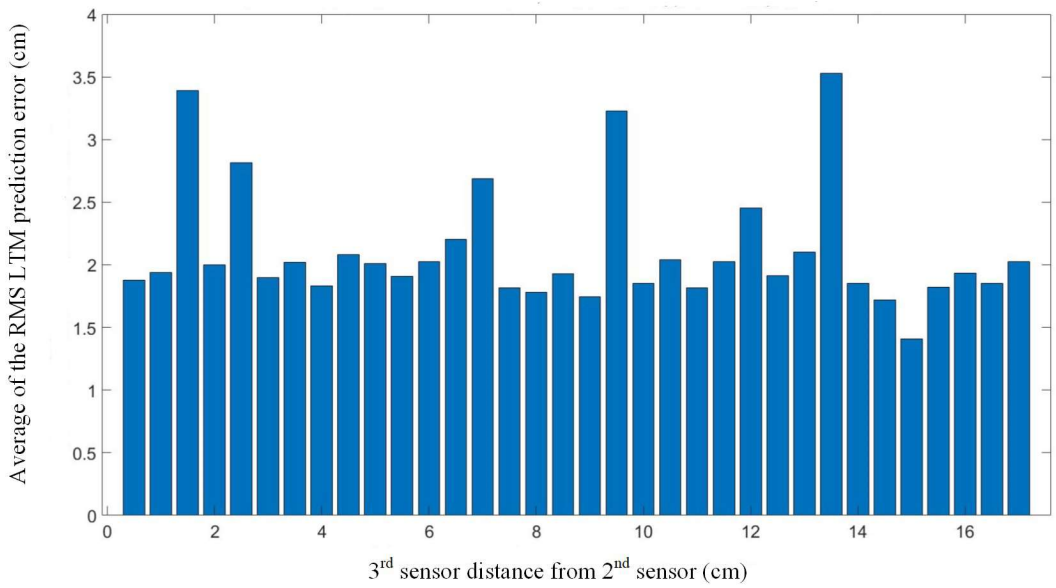

Fig. 5.4: Average of the RMS LTM prediction error when only the 3rd sensor is moving from the 2nd sensor and the 1st sensor is fixed (15 cm away from the 2nd sensor); number of neurons used for training is two/hidden layer

calculated for this structure by moving the structure in both directions. The same process was continued to calculate the average of the RMS LTM estimation error where only the 3rd sensor was being moved every half cm up to 17 cm (downwards along the Y-axis). Fig 5.2 demonstrates that the overall average of the RMS LTM estimation error has increased when only the 3rd sensor is moving compared to the structure when both the 1st and the 3rd sensors were moving symmetrically. It also shows the average of the RMS LTM prediction error is lowest when the 3rd sensor is 15 cm away from the 2nd sensor, evidencing that the estimation of LTM works best when the sensor position is symmetrical. For this reason, this symmetrical structure for the sensors was used for ANN training where both the 1st sensor and the 3rd sensor was chosen 15 cm apart from the 2nd sensor, which was positioned in the middle of the cart. For the training and testing of the ANN algorithm, ANSYS magnetic field data were smoothed and curve fitted to eliminate the impact of final accuracy of the ANSYS simulation. As a result, the difference between the average of the RMS LTM prediction error for different sensor positions is relatively low.

It has been already discussed how the number of ANN neurons affects the estimation of LTM. For the calculation presented in Fig 5.2, the number of delays is selected to be ten, as well as the number of neurons. Fig 5.3 represents how the estimation error changes for different positions of the 3rd sensor when the number of neurons is reduced to four. As one can see, the averages of the RMS LTM prediction errors have increased for all positions of the 3rd sensor. Fig 5.4 shows the average of the RMS LTM estimation error when the number of delays is ten and the number of neurons is two. It is evident from the graph that the overall estimation error has increased further for every 3rd sensor position. However, from all three bar graphs, it is evident that the average of RMS LTM prediction error is lowest when the 3rd sensor is 15 cm away from the 2nd sensor, or in other words, when the overall sensor structure is symmetrical.

5.2.2 Sensor Positions with Different Angles

After the selection of the lateral position of the sensors, the angle between the sensor and X-axis was varied to measure the average of the LTM prediction error to evaluate the

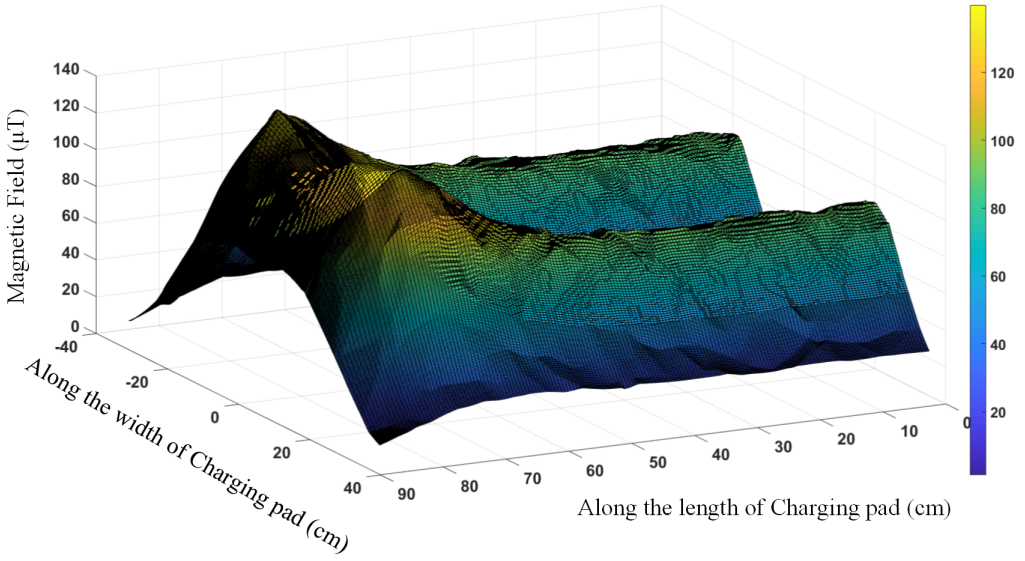

Fig. 5.5: Magnetic field along the charging pad for simulation when angle between X axis and sensor is 30 degree.

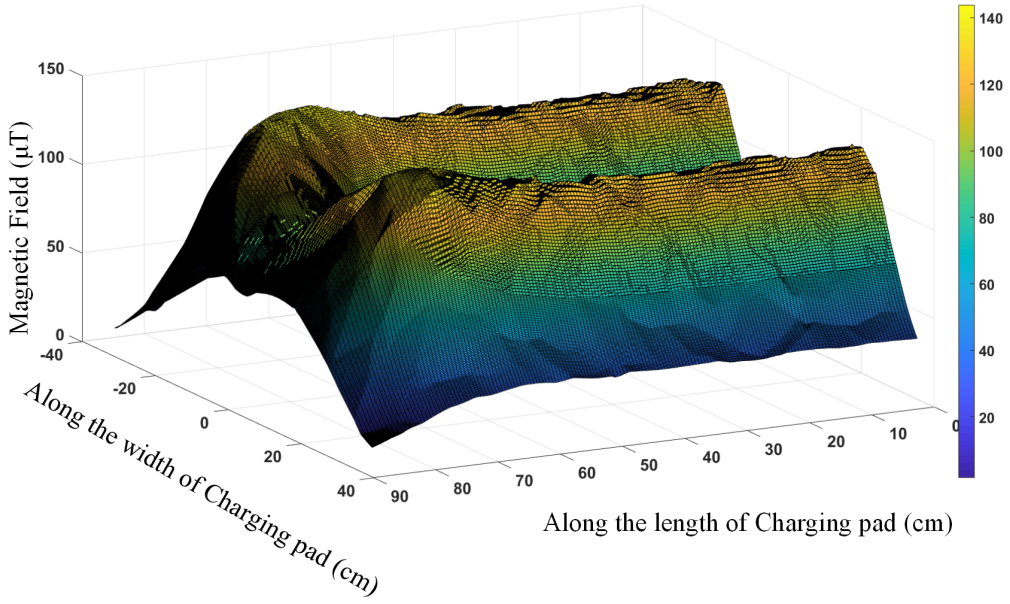

Fig. 5.6: Magnetic field along the charging pad for simulation when angle between X axis and sensor is 45 degree.

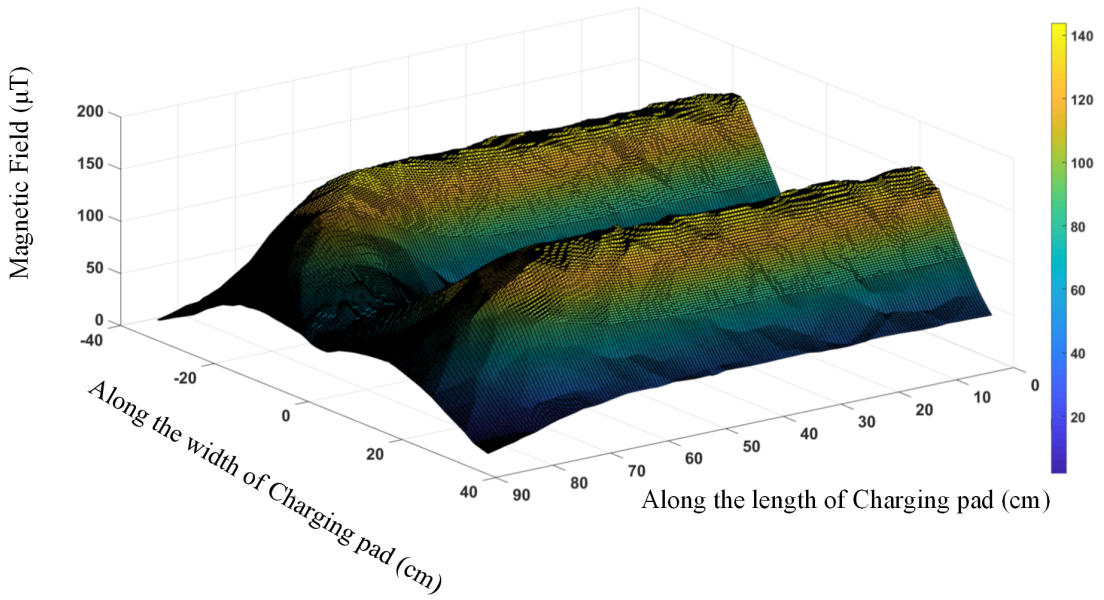

Fig. 5.7: Magnetic field along the charging pad for simulation when angle between X axis and sensor is 60 degree.

Angle between X axis and sensor (degree)	Average of the RMS LTM prediction error (cm)
0	0.3234
30	0.4239
45	0.6138
60	0.3932
90	0.3187

Table 5.2: List of Average of the RMS LTM prediction error for different angle between X axis and sensor

Vehicle-Sensor Distance (cm)	Average of RMS LTM Prediction Error (cm)
2	0.3237
3	0.4112
4	0.3962
5	0.3632

Table 5.3: List of the Average of RMS LTM Prediction Error for different Vehicle-Sensor Distances

effect on ANN LTM estimation. The simple formula was used to calculate the magnetic field, B=Bx*$Cos(\theta)$+By*$Sin(\theta)$, where θ = angle (in degree) between X-axis and the sensor. From the equation, it is clear that when $\theta = 0°$, magnetic field (B) is equal to Bx. In a similar way magnetic field (B) is equal to By, when $\theta = 90°$. If the angle increases up to $\theta = 45°$, Bx has more influence than By on the total magnetic field. When the angle is increased from 45° to 90° impact of By is more prevalent than Bx. Fig 5.5, Fig 5.6, Fig 5.7, illustrates the influence of Bx and By on total magnetic field throughout the charging pad when angle is 30°, 45° and 60° respectively. Table 5.2 shows average of the RMS LTM prediction error for different angles from 0° to 90°. From this table, it is clear that error is lowest when only By is considered for the average of the RMS LTM prediction error calculation. But using only Bx provides the sense of EV position as the sensor can detect the big hump of the magnetic field (Fig 4.3) and has the 2nd least average of RMS LTM prediction error. It is also noticeable that error starts to increase when the theta increases and the mean of RMS LTM estimation error is highest when theta is 45°. The error starts to decline when the angle is further increased and become lowest when the sensor is parallel to the Y-axis. When the angle is between 0° and 90°, the magnetic field has the effect of both Bx and By. This effects the structure of the magnetic field curves and curve fitting becomes difficult for every region as the pattern is different for the different region compared to the curves for By and Bx. Since the use of only Bx has the advantage of EV position sensing and the average LTM prediction error is comparatively low, only Bx was used for the final ANN algorithm.

5.2.3 Selection of the Vehicle-Sensor Distance

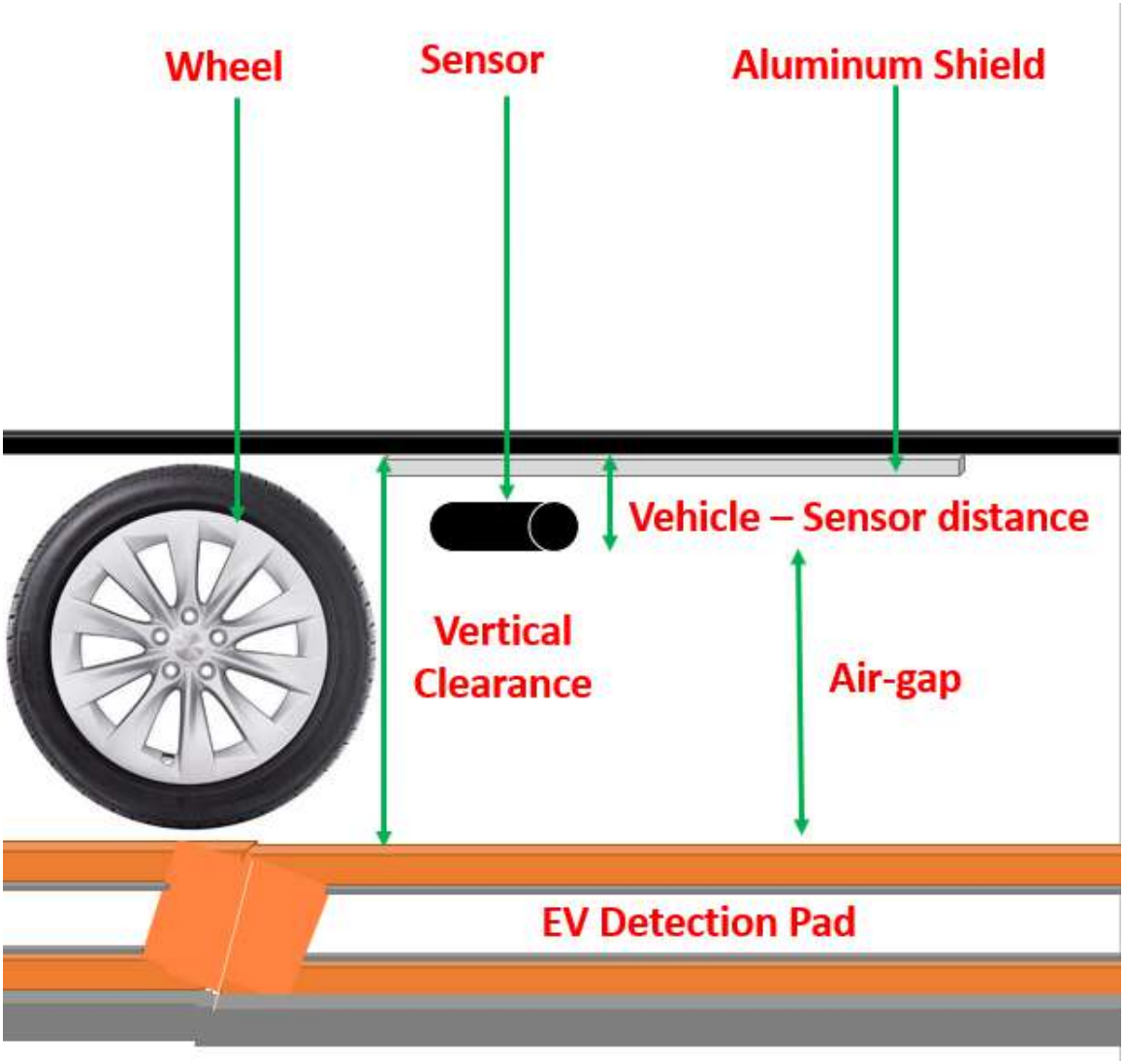

Fig. 5.8: Visualization of Vehicle-Sensor Distance and vertical clearance

After the selection of sensor lateral position and angle with the X-axis, Vehicle-Sensor Distance was selected. (Fig 5.8) shows the relationship of the Vehicle-Sensor Distance, Air-gap, and Vertical Clearance. Vehicle-Sensor Distance is the distance between the car bottom (from the surface of the Aluminum Shield) and the center of the sensor. The Air-gap is the distance between the middle of the sensor and charging coil, where vertical clearance is equal to the summation of Vehicle-Sensor Distance and Air-gap. For Different EVs, the vertical clearance would be different, but the distance between sensor and EV bottom would be fixed. To calculate the best Vehicle-Sensor Distance position, the magnetic field was taken for different Air-gaps where the Vehicle-Sensor Distance was maintained the same. Then the mean of RMS LTM estimation error was calculated for that specific Vehicle-Sensor Distance including different Air-gap positions and the whole procedure was repeated for a few other Vehicle-Sensor Distances. Fig 5.8 illustrates different combinations of Vehicle-Sensor Distance and Air-Gap that were used to evaluate the best Vehicle-Sensor Distance for ANN implementation. Table 5.3 shows average of RMS LTM prediction error for corresponding Vehicle-Sensor Distance.

5.3 Effects of Speed on Estimation of LTM

In this section, the effect of speed on the estimation of LTM is discussed. In the previous analysis, the sampling rate was constant at 250 μs. Since the sampling rate is constant, if the speed increases, the number of the data point for ANN estimation will decrease. If the speed becomes double, then the number of data points will be reduced to half, comparing to the data points for the previous speed. Fewer data points mean ANN prediction error would also increase. Total of twelve combinations of speed was considered to examine how much speed affects ANN LTM estimation where the speed range was 0.25 m/s to 3 m/s. Fig 5.9 shows how the average of the RMS LTM estimation error has changed for different speeds. It is evident from the figure that the average of RMS LTM prediction error is lowest for 0.25 m/s since it has the highest number of data points and ANN could predict more accurately. For the same reason, the average of the RMS LTM estimation error is highest when the speed is 3 m/s. But the overall average of the RMS LTM estimation error was

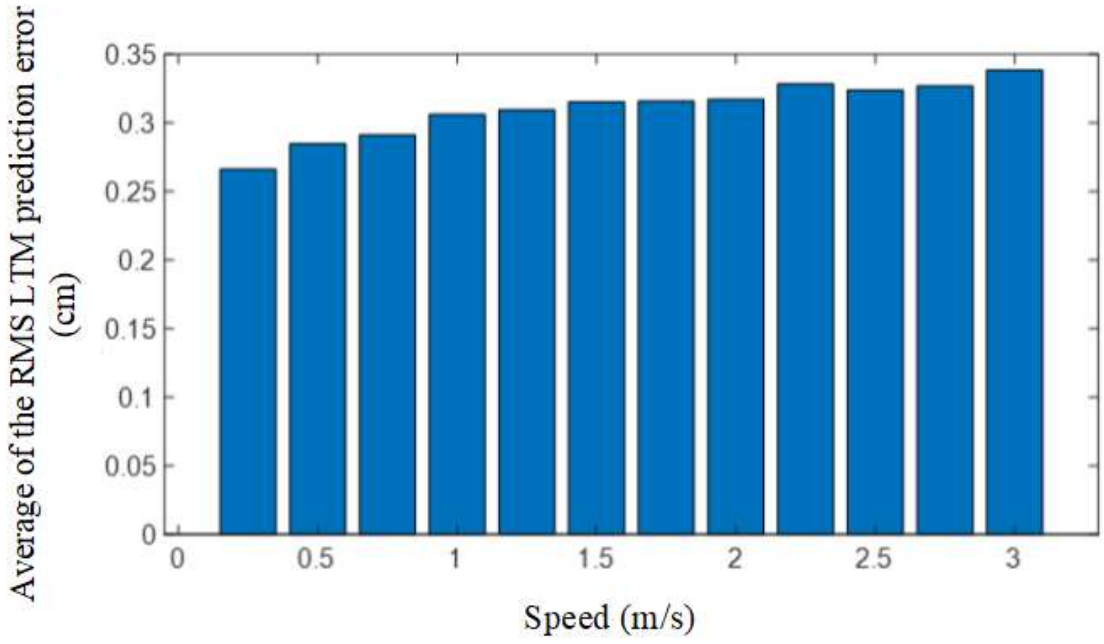

Fig. 5.9: Average of the RMS LTM prediction error for different speeds.

less than 0.35 cm.

In this project, to predict LTM for different speeds, ten neurons/layer and ten delays had been used. One concerning factor to be considered here to predict the LTM when EV has higher speed since the average of the RMS LTM prediction error slightly increases due to less number of data input. It has been already demonstrated in Table 5.1 that decrements in the number of neurons to train ANN, causes an increment in error in the estimation of LTM. On the other hand, error in the estimation of LTM increases very slightly when the number of delays is lessened. Since both, the number of neurons and the number of delays generate the same number of coefficients in the training process, reducing the number of delays and increasing the number of neurons can produce more accurate results for the estimation of LTM with higher speed.

5.4 Results for Vertical Clearance Detection

Estimation of Vertical Clearance is necessary since the magnitude of the magnetic field will vary for different heights for the same position of the charging pad, which will result in

Vertical Clearance (cm)	speed (m/s)					
11	0.5	1	1.5	2	2.5	3
12	0.5	1	1.5	2	2.5	3
13	0.5	1	1.5	2	2.5	3
14	0.5	1	1.5	2	2.5	3
15	0.5	1	1.5	2	2.5	3

Table 5.4: Speeds and Combination of Vertical Clearances used for ANN Training to calculate the mean of RMS LTM estimation error

Vertical Clearance (cm)	speed (m/s)					Average VC Prediction Error (cm)
11.5	0.75	1.25	1.75	2.25	2.75	.180
12.5	0.75	1.25	1.75	2.25	2.75	.176
13.5	0.75	1.25	1.75	2.25	2.75	.129
14.5	0.75	1.25	1.75	2.25	2.75	.154

Table 5.5: Speeds and Combination of Vertical Clearances used for ANN Estimation Purposes

the poor estimation of LTM. Since different EVs might have different Vertical Clearances, it is important for ANN to predict Vertical Clearance so that it can predict LTM more precisely. For training purposes, ANN was trained for five different Vertical Clearances between 11 cm to 15 cm in incremental steps of 1 cm. For each Vertical Clearance position, ANN was trained for six different speeds between 0.5 m/s to 3 m/s in incremental steps of 0.5 m/s. Table 5.4 illustrates different combinations of different Vertical Clearances and speeds for training ANN to estimate Vertical Clearances.

For estimation of Vertical Clearances, the magnetic field of different Vertical Clearances was chosen. For testing ANN, the network was tested with four different Vertical Clearances between 11.5 cm to 14.5 cm in incremental steps of 1 cm. For each Vertical Clearance position, ANN was tested for five different speeds between 0.75 m/s to 2.75 m/s in incremental steps of 0.5 m/s. That five different speeds were used in testing ANN, were not included in the training ANN phase. For testing of the prediction algorithm, the average of Vertical Clearance prediction error was calculated for each speed. Average of Vertical Clearance prediction error for a specific speed was calculated in the same way the average of RMS LTM prediction error was calculated. Then each estimated error for the five different

speeds was averaged to calculate the ultimate average of the Vertical Clearance prediction error for that corresponding Vertical Clearance. Table 5.5 shows mean of Vertical Clearance prediction error for different Vertical Clearances. In each case, the average error was very low, less than 2 mm, which proves that ANN can successfully predict the VC with a very good accuracy.

CHAPTER 6

FUTURE WORKS

As this project is part of a larger design (Toyota Dynamic Wireless Wireless Power Transfer System), there is much work that must be completed for this project to be considered complete. This project is only the first stage of the three phases. The very next step will be to design the hardware of the simulation design for the first stage.

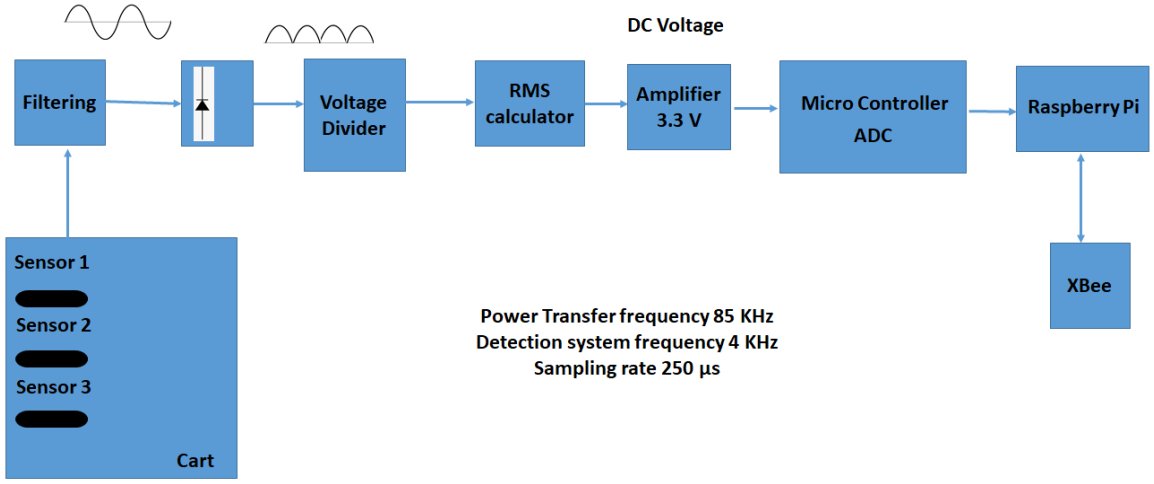

Fig. 6.1: Block diagram of the complete hardware system.

Fig 6.1 demonstrates the block diagram of the hardware implementation part for the simulation of EV-based LTM detection system. The block diagram starts with three sensors connected on a cart which will be attached to the front of a car model. Fig 6.2 shows a proper sensor structure on the cart. The model of the cylindrical shaped sensor is MC90R. Each sensor is 15 cm apart from each other where the second sensor is situated in the middle of the cart (along the Y-axis). The sensors can move laterally, providing flexibility on the selection of a specific lateral position. The cart has four wheels on it so that it can be smoothly pushed by the car model. The car will push forward the cart, and the sensors on the cart will measure the magnitude of the magnetic flux density along the EV detection

charging pad.

Fig 6.3 illustrates the PCB design for the hardware controller system. The sensors will generate ac voltage signals depending on the intensity of the magnetic field. Then the rectifier diodes will be introduced to convert the AC signal to a DC signal with the help of the RMS calculator. Then the DC signal will be amplified using an op-amp to a 3.3-level signal to be used in the micro-controller. The sampling rate for the micro-controller is 250 μs. Then raspberry pi will be used for the computation needed to predict the LTM and Vertical Clearance. Xbee will be used for communication between the controller and the model car, and uploading the data online. Here, the detection system frequency will be used as 4 KHz, and the power transfer frequency will be around 85 KHz.

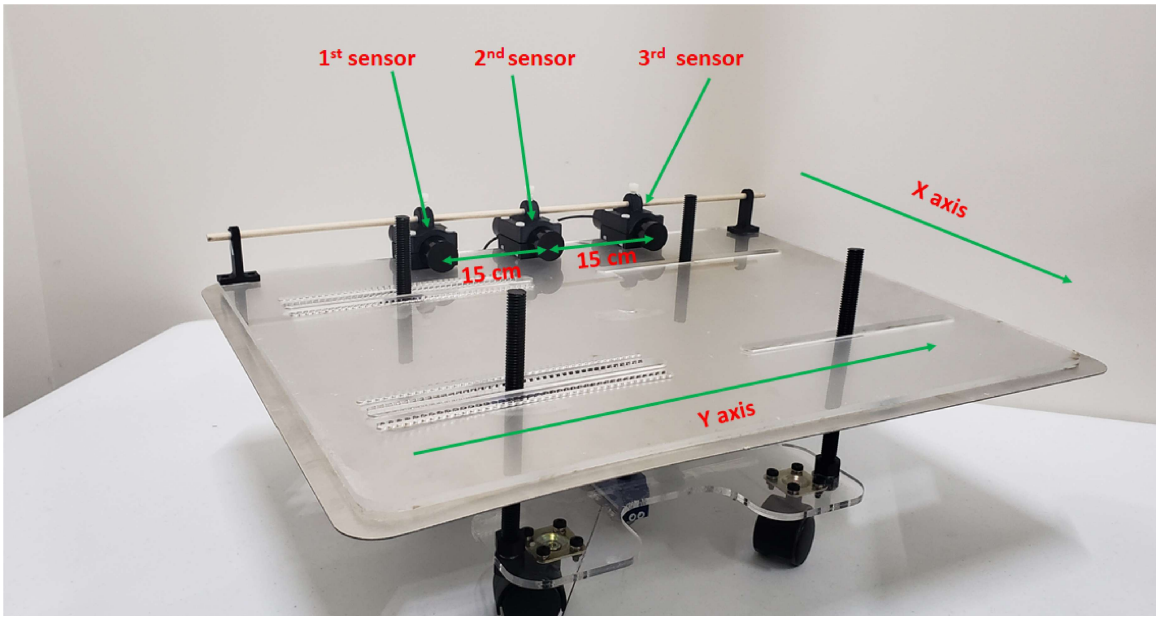

Fig. 6.2: Sensor positions on cart.

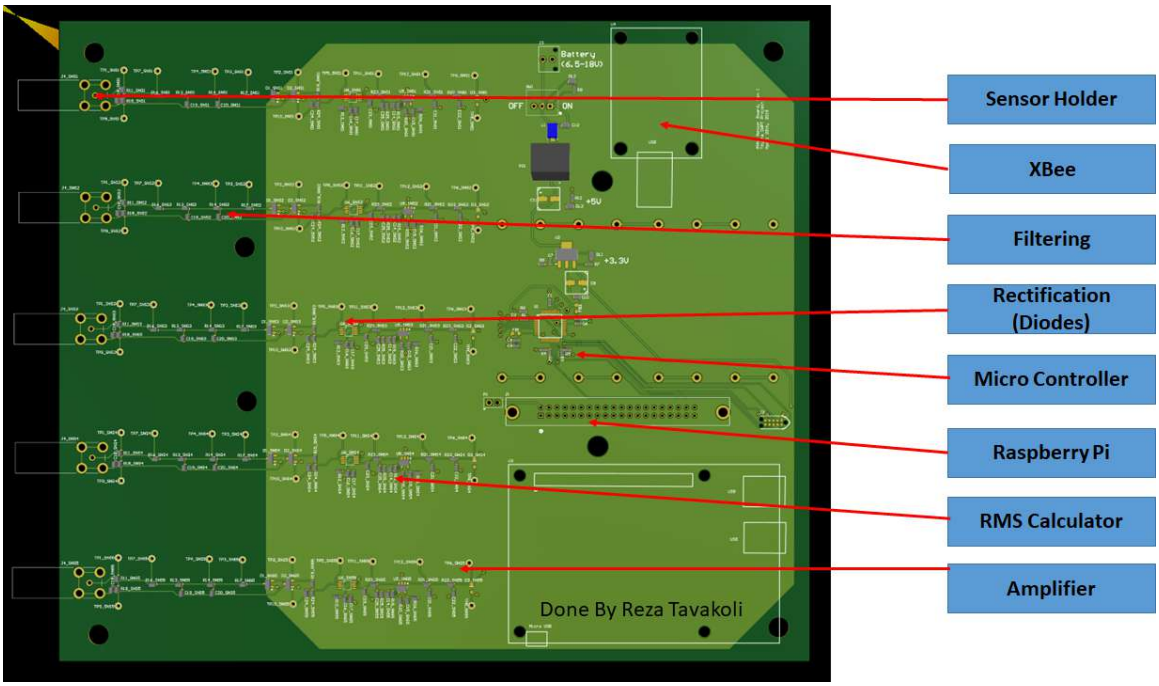

Fig. 6.3: PCB design for the controller.

CHAPTER 7

CONCLUSION

Object detection using magnetic field is continuously being experimented and modified for different implementations. This research concept is implemented to improve the efficiency of wireless charging as the efficiency heavily depends on the proper alignment of the vehicle with respect to the transmitter coil. This result will help to overcome the reduction of the wireless power transfer due to lateral misalignment. The proposed solution can be integrated into autonomous vehicles, Driver Information Systems (DIS), Intelligent Transportation Systems (ITS), etc., by modifying it for different heights and speeds of a dynamically charged vehicle. In addition, this concept can be implemented in traffic controlling systems by using it for vehicle lane detection. Another significant feature of the proposed solution is that the installation of the sensors is easy and can be implemented at low cost. The hardware implementation will confirm the effectiveness of the simulated results.

REFERENCES

[1] B. Fleming, "Electric vehicle collaboration-toyota motor corporation and tesla motors [automotive electronics]," *IEEE Vehicular Technology Magazine*, vol. 8, no. 1, pp. 4–9, March 2013.

[2] S. A. Birrell, D. Wilson, C. P. Yang, G. Dhadyalla, and P. Jennings, "How driver behaviour and parking alignment affects inductive charging systems for electric vehicles," *Transportation Research Part C: Emerging Technologies*, vol. 58, pp. 721–731, 2015.

[3] M. A. Clark, "Induction loop vehicle detector," Feb. 4 1986, uS Patent 4,568,937.

[4] G. R. Nagendra, L. Chen, G. A. Covic, and J. T. Boys, "Detection of evs on ipt highways," *IEEE journal of emerging and selected topics in power electronics*, vol. 2, no. 3, pp. 584–597, 2014.

[5] Y.-K. Ki and D.-K. Baik, "Vehicle-classification algorithm for single-loop detectors using neural networks," *IEEE Transactions on Vehicular Technology*, vol. 55, no. 6, pp. 1704–1711, 2006.

[6] Q. Wang, J. Zheng, B. Xu, and Y. Huang, "Analysis and experiments of vehicle detection with magnetic sensors in urban environments," in *Cyber Technology in Automation, Control, and Intelligent Systems (CYBER), 2015 IEEE International Conference on*. IEEE, 2015, pp. 71–75.

[7] R. Tavakoli and Z. Pantic, "Ann-based algorithm for estimation and compensation of lateral misalignment in dynamic wireless power transfer systems for ev charging," in *Energy Conversion Congress and Exposition (ECCE), 2017 IEEE*. IEEE, 2017, pp. 2602–2609.

[8] J. Shin, S. Shin, Y. Kim, S. Lee, B. Song, and G. Jung, "Optimal current control of a wireless power transfer system for high power efficiency," in *Electrical Systems for Aircraft, Railway and Ship Propulsion (ESARS), 2012*. IEEE, 2012, pp. 1–4.

[9] S. Shin, J. Shin, B. Song, S. Lee, Y. Kim, G. Jung, and S. Jeon, "Wireless power transfer system for high power application and a method of segmentation," in *Wireless Power Transfer (WPT), 2013 IEEE*. IEEE, 2013, pp. 76–78.

[10] R. Tavakoli and Z. Pantic, "Analysis, design, and demonstration of a 25-kw dynamic wireless charging system for roadway electric vehicles," *IEEE Journal of Emerging and Selected Topics in Power Electronics*, vol. 6, no. 3, pp. 1378–1393, 2018.

[11] A. Azad, A. Echols, V. Kulyukin, R. Zane, and Z. Pantic, "Analysis, optimization, and demonstration of a vehicular detection system intended for dynamic wireless charging applications," *IEEE Transactions on Transportation Electrification*, 2018.

[12] K. Gurney, *An introduction to neural networks*. CRC press, 2014.